Three-dimensional modeling of the 1983-1984 eruption at Piton de la Fournaise Volcano, R6union Island

Valérie Cayol, François H Cornet

JOURNAL OF GEOPHYSICAL RESEARCH, VOL. 103, NO. B8, PAGES 18,025–18,037, AUGUST 10, 1998

Three-dimensional modeling of the 1983-1984 eruption at Piton de la Fournaise Volcano, Réunion Island

Valérie Cayol and François H. Cornet

Institut de Physique du Globe de Paris, Paris

Abstract. Displacement vectors on 125 points over a 6-km^2 area were calculated [*Zlotnicki et al.*, 1990] for Piton de la Fournaise volcano, Réunion Island, from photogrammetric surveys conducted in September 1981 and again in September 1984. An eruptive crisis with two episodes occurred during the 3 years between the surveys. We modeled the displacements from the photogrammetric surveys using a three-dimensional mixed boundary element method. The model shows that both eruptive episodes were fed by a single dike oriented 165° from north. As the dike approached the ground surface, it divided into segments that rotated into an en echelon pattern. The model that best fits all observations suggests that the stress state within the volcano is quasi-isotropic such that horizontal stresses equal the overburden. These high horizontal stresses are incompatible with an elastic edifice loaded merely by gravitational forces. However, they may be attributed to the cumulative effect of repeated dike intrusions.

1. Introduction

Most deformation models of volcanoes suppose that the Earth is a linear, elastic, isotropic, and homogeneous half-space and that the sources of deformation have simple shapes, such as spheres [*Mogi*, 1958; *McTigue*, 1987], ellipsoids [*Davis*, 1986; *Dieterich and Decker*, 1975], or rectangular planes [*Okada*, 1985]. These approximations can lead to erroneous interpretations of the deformation data. Indeed, the mechanical response of volcanoes can be significantly affected by several complexities that are omitted altogether by these simple models.

1.1. Geometrical Complexities

The rock mass of volcanoes is cut by major discontinuities along which deformations localize. Dikes are a major structure for transporting magma to the ground surface [*Chadwick and Dieterich*, 1995], and shear fractures sometimes critically affect the deformation field of volcanoes [*Pollard et al.*, 1983]. Therefore mechanical models of volcanoes should allow for fractures, whether tensile or shear.

Magma is stored in reservoirs. In deformation models, these reservoirs are often idealized as having very simple geometry [*Mogi*, 1958; *Davis*, 1986]. However, seismic refraction studies [*Hill and Zucca*, 1987] sometimes indicate more complex shapes which should also be incorporated in analyses.

Paper number 98JB00201.
0148-0227/98/98JB-00201$09.00

1.2. Interaction Between Structures

In eruptions, different structures often interact. For instance, magma reservoirs can feed dikes, displacements on a fault can induce displacements on another fault, etc. Very often in modeling studies, deformations and stresses created by various sources are superposed using different well-known analytic deformation models (for instance, *Mogi*'s [1958] point source model and *Okada*'s [1985] fracture model). This should be done with caution, because the approximation that the influence of one deformation source on another is negligible can only be done provided these structures are far enough from each other.

1.3. Topographic Effects

Volcanoes, being agents of mountain building, are often associated with considerable topographic relief. For ridges, *McTigue and Segall* [1988] showed that a slope of 20° implies ground surface displacements that are at some points 40% smaller than those associated with a flat ground surface. For volcanoes, *Cayol and Cornet* [1998] showed that neglecting topography can result in an overestimation of the source overpressure. For an average slope of the volcano of 30°, this overestimation can be as high as 50%. Additionally, magma reservoirs are sometimes located at shallow depth inside edifices, and simple symmetries of volcanoes can rarely be assumed. For quantitative interpretation of the elastic deformation field of most volcanoes, it is therefore important to use fully three-dimensional modeling methods.

1.4. Boundary Conditions

Dikes are often subvertical. This implies that regional stresses that act through the dike walls, as well as the magma pressure, vary with height. These variations should be considered.

In the work presented here, the complexities taken into account are the geometrically complex deformation sources and the topography. With our modeling method, these sources can be dikes, faults, or magma reservoirs, and they can interact. We use static analysis because static models are suitable for the interpretation of deformation data that are discontinuous in time. The rock mass is assumed to be linearly elastic. Indeed, deformation processes that most commonly affect volcanoes, fissure eruptions or inflations of magma reservoirs, are associated with small displacement gradients, which imply that the medium does, indeed, behave elastically. In this study, differences in volcanic products and temperature distributions are neglected, so that the rock mass is assumed to be homogeneous and isotropic. Finally, the imposed boundary conditions are stresses, as it is more appropriate to impose stresses than displacements on fractures [*Zeller and Pollard*, 1992]. Our method permits imposing two types of perturbations: overpressures acting on tensile fractures and reservoirs, and shear stress drops on faults.

As we intend to model realistic boundaries, a numerical boundary element method is used. For the problems we address, this method is numerically more efficient than the finite element method for the following reasons: First, we are mainly interested in calculating boundary displacements [*Murkherjee and Marjoria*, 1984]. Second, with boundary element methods, far-field boundary conditions are implicitly taken into consideration, so that remote boundaries do not have to be defined. Moreover, boundary elements permit modification of model geometries with reduced supplementary calculations.

The first part of this paper reviews the principles of the three-dimensional (3-D) mixed boundary element (BE) method developed for the analysis of deformation and stress fields of volcanoes. The second part of the paper deals with the analysis of the 1983-1984 eruptive crisis of Piton de la Fournaise. For this eruption, a dense set of ground surface displacements calculated by photogrammetry is available. This displacement field is analyzed using the 3-D mixed BE method. The geometry and position of the sources of deformation as well as the overpressure distributions are determined.

2. Three-Dimensional Mixed Boundary Element Method

Boundary element methods are based on the approximation of the boundaries of a body by a finite number of elements and on the use of known analytical solutions to singular boundary value problems. Provided the governing partial differential equations of the physical problem are linear, the analytical solutions can be added to satisfy the boundary conditions at each element in more complex problems.

The 3-D mixed BE method [*Cayol and Cornet*, 1997] combines two of the most widely used boundary element methods of linear elasticity: the direct method [*Lachat and Watson*, 1976] and the displacement discontinuity method [*Crouch*, 1976]. Indeed, the two methods are complementary; the direct method possesses a lower mathematical singularity than the displacement discontinuity method, making the direct method more efficient and exact for modeling structures such as ground surfaces or pressurized reservoirs but not fractures, whereas the displacement discontinuity method is the most suitable for fractures. In the problem addressed here, tractions are the specified boundary values.

Following *Diering* [1981], the mixed method is derived from Betti's reciprocal theorem and the solution to Kelvin's problem of a point load in an infinite body. Betti's reciprocal theorem is written for a body with nonfracture boundaries Γ_M (referred to as a massive boundary) and closed fractures Γ_F such that opposite sides are at the same location. Fractures are then assumed to correspond to jumps in displacements and continuous tractions, and the boundaries of the body are discretized with triangular elements. To improve efficiency, the variations of displacements and tractions are considered to be constant for fracture elements with their calculation points at the elements centroid; for massive boundaries they are considered linear with their calculation points located at the elements apexes. These approximations result in N_M massive boundary elements and N_F fracture elements with N_L and N_F calculation points on massive boundaries and fractures, respectively. Finally, the following linear system of equations is obtained,

$$\mathbf{L}\,\mathbf{X} = \mathbf{R}, \tag{1}$$

where $\mathbf{L}$ is the influence coefficient matrix, consisting of integrals to the solution of Kelvin's problem, $\mathbf{X} = \{\mathbf{u}^1 \ldots \mathbf{u}^{N_L}\mathbf{d}^1 \ldots \mathbf{d}^{N_F}\}^T$ represents the unknown massive boundary displacements and fracture displacement discontinuities, and $\mathbf{R}$ is a known vector that incorporates the traction boundary conditions.

This system is solved for $\mathbf{X}$, and displacements at any point ψ inside the body can be calculated using Somigliana's identity written for boundaries with both massive boundaries and fractures,

$$\mathbf{u}^\psi = -\mathbf{H}^\psi\,\mathbf{X} + \mathbf{G}^\psi\,\mathbf{P}, \tag{2}$$

where $\mathbf{H}^\psi$ and $\mathbf{G}^\psi$ are influence coefficient matrices, and $\mathbf{P} = \{(\mathbf{p}^{11}\mathbf{p}^{21}\mathbf{p}^{31})^T \ldots (\mathbf{p}^{1e}\mathbf{p}^{2e}\mathbf{p}^{3e})^T \ldots (\mathbf{p}^{1N_M}\mathbf{p}^{2N_M}$

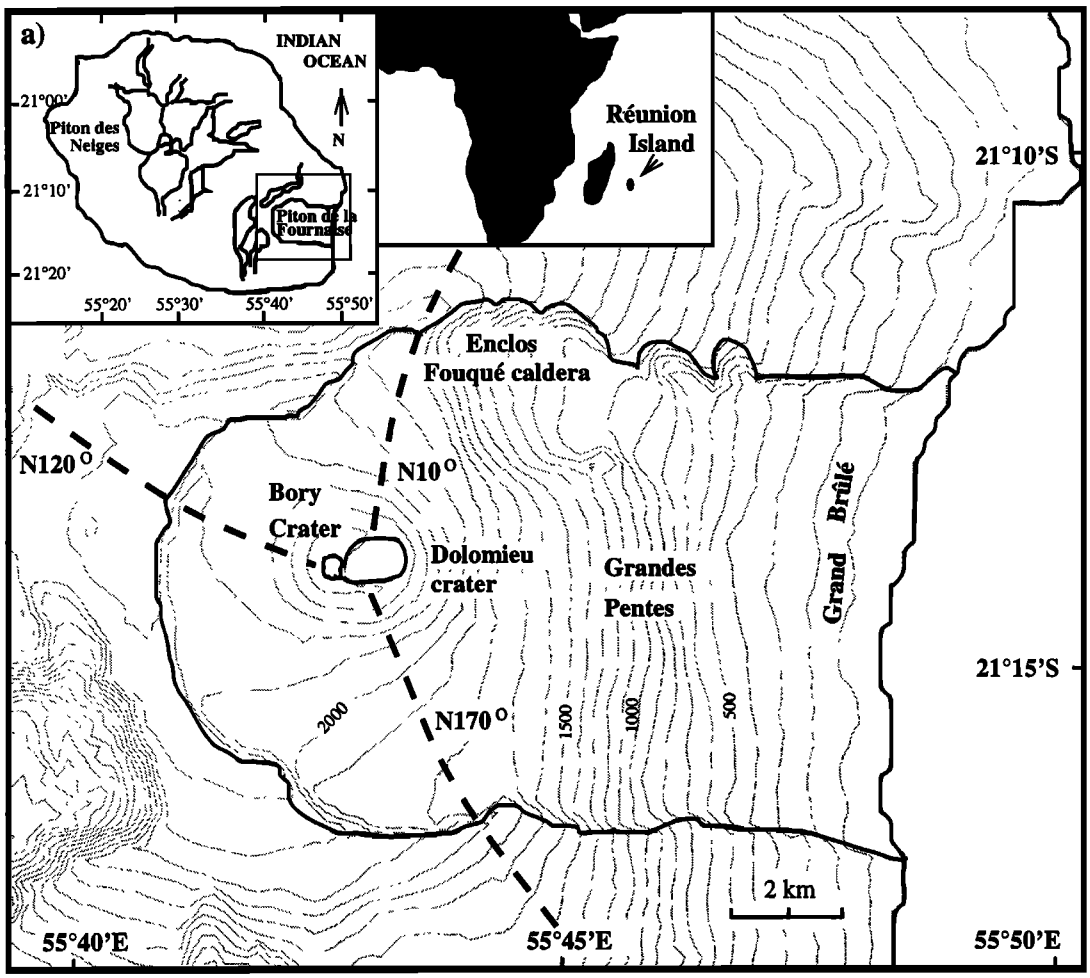

Figure 1. (a) Réunion Island (b) Main structures of Piton de la Fournaise volcano. Bold dashed lines indicate locations of main fracture zones; bold solid lines are the craters and caldera outlines. Elevation contours are every 100 m.

$\mathbf{p}^{3N_M})^T\}$ is the traction vector on every node of the N_M elements of the massive boundaries.

Differentiating this equation and using Hooke's law gives stresses at point ψ,

$$\sigma^{\psi} = -\mathbf{S}^{\psi}\,\mathbf{X} + \mathbf{R}^{\psi}\,\mathbf{P}. \tag{3}$$

The 3-D mixed BE method has been implemented from the preexisting program COMPUTE^{3D} [*Curran et al.*, 1994] based only on the direct method. Numerical implementation of the mixed BE method for analyzing volcanic structures requires various numerical treatments [*Cayol and Cornet*, 1997]. One of them deals with the calculation of influence coefficients on nonclosed surfaces like the ground surface. This problem is solved introducing a virtual surface that complements the ground surface. Another numerical difficulty concerns the intersection of massive boundaries with fractures. This problem is overcome by making constant every element belonging to a massive boundary adjoining a fracture.

3. Analysis of the Deformation Field Associated With the 1983-1984 Eruption of Piton de la Fournaise Volcano

Piton de la Fournaise (Figure 1) is a basaltic shield volcano on which most eruptions occur along eruptive fissures in the central cone area. Geological and geophysical data indicate the presence of a shallow reservoir composed of magma pockets [*Lénat and Bachèlery*, 1990; *Bureau et al.*, 1998]. This reservoir is probably located between 500 and 1300 m below the summit craters of the volcano. Eruptions since 1977 are interpreted to be fed by a larger crystallizing reservoir located below sea level [*Lénat et al.*, 1989b; *Sapin et al.*, 1996; *Albarède*, 1993]. The nature of the connection between the deeper reservoir and the shallow reservoir is unknown.

In September 1981 and June 1984, two photogrammetric surveys [*Zlotnicki et al.*, 1990] were carried out at Piton de la Fournaise. Using the photogrammetric method developed by Institut Géographique National [*Corre and Giraudin*, 1982], displacement vectors were

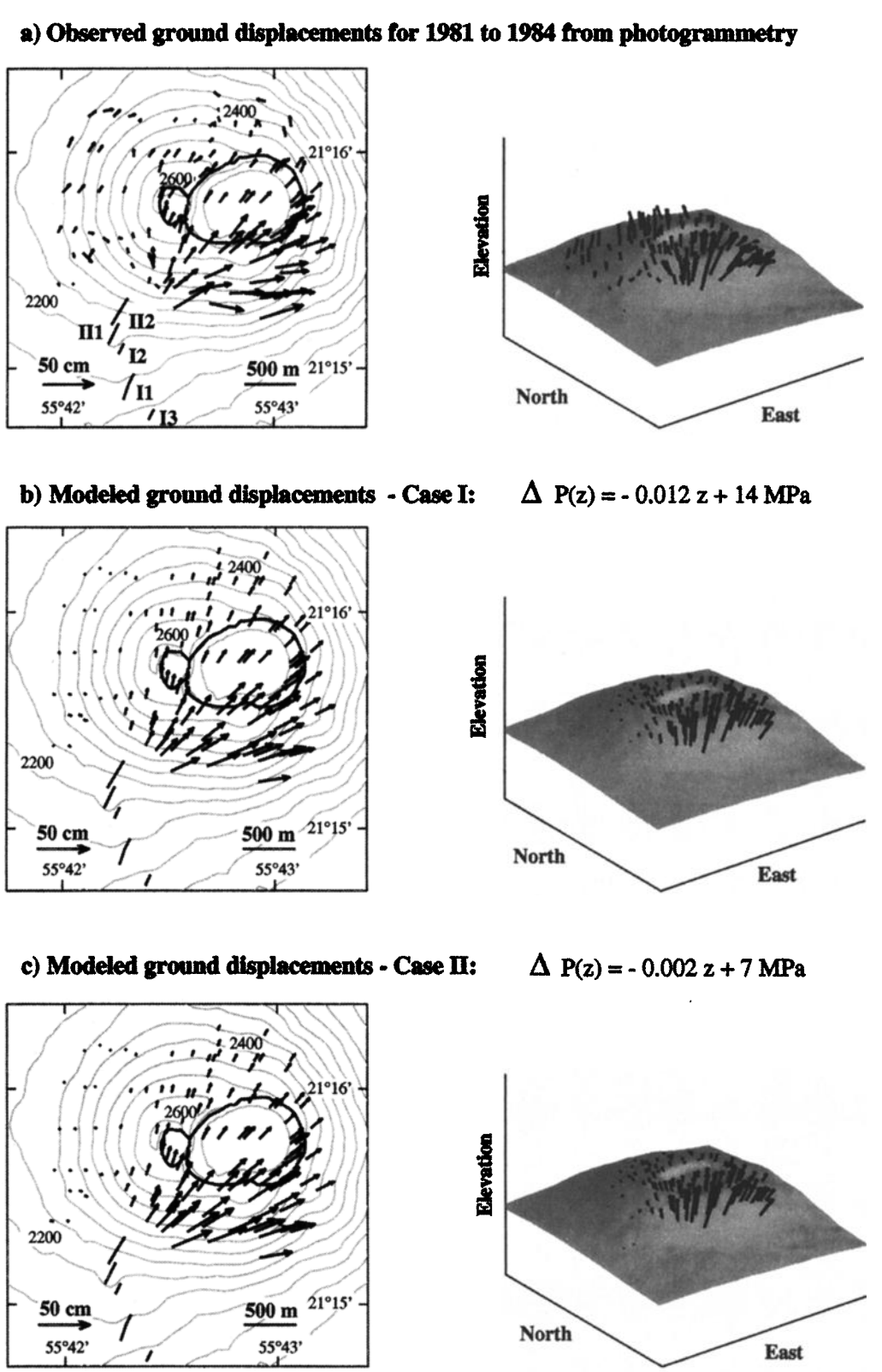

Figure 2. Comparison between observed ground displacements and modeled ground displacement calculated by the three-dimensional mixed boundary element (BE) method. Figures on the left are map views with 50-m-elevation contours. Figures on the right are oblique perspectives. (a) Displacement vectors calculated from the photogrammetric surveys of September 1981 and June 1984. Uncertainties on displacements are 3 cm. I1, I2, and I3 are the eruptive fissures of the first episode of the eruption, and II1 and II2 are the eruptive fissures of the second episode. (b) Displacements computed by the mixed boundary element method for a dike with an overpressure $\Delta P(z) = (-0.012z + 14)$ MPa. The elastic medium has a density of 2500 kg/m^3, and the dike is filled with a magma of density equal to 2650 kg/m^3, Young's modulus is 5 GPa, and Poisson's ratio is 0.25. (c) Displacements computed by the mixed BE method for a dike with an overpressure $\Delta P(z) = (-0.002z + 7)$ MPa.

calculated at 125 points over a 6-km^2 area (Figure 2a). Displacements as large as 50 cm southwest of the central cone were recorded with uncertainties of only 3 cm. During the 3-year period, only one eruptive crisis with two episodes occurred [*Lénat et al.*, 1989a]. It lasted from December 4, 1983, to the end of February 1984 and had vents located on the southwestern flank of the central cone (Figure 2a).

Deformations associated with this eruption were also recorded by an extensometer located in Bory crater and by clinometric and geodetic stations [see *Lénat et al.*, 1989a, Figures 6 and 8]. These measurements indicate that very little deformation occurred between October 1981 and the beginning of the eruption and between the end of the eruption and December 1984. Thus the deformations observed by photogrammetry can be mostly attributed to the 1983-1984 eruption.

Because the photogrammetric data are very dense and accurate, they are particularly well suited to a precise determination of the characteristics of the source of deformation. Using rectangular dislocations in a homogeneous elastic half-space [*Okada*, 1985], *Zlotnicki et al.* [1990] modeled this displacement field and showed that it could be explained by a shallow dike intrusion. With dislocation models, displacements are the imposed boundary condition, and the mechanical interactions between different fractures are ignored. As we have explained in the introduction, these simplifications can lead to erroneous results. Moreover, the eruption occurred in the summit area of the volcano where topographic relief is significant (average slope of 15°-20°). As this eruption is fissural, an axisymmetrical model is improper. Below, the eruption is analyzed using the 3-D mixed BE method. A realistic topography of the ground surface is taken into account.

3.1. Parameters of the Preliminary Model

3.1.1. Mechanical properties of the elastic medium. The density of the elastic medium is estimated at 2500 kg/m^3, a value measured from borehole samples. In situ elastic coefficients at a length scale of a few hundred meters are estimated using seismic wave velocities. A dynamic Young's modulus of E_d = 20 GPa and a dynamic Poisson's ratio of $\nu_d = 0.25$ are determined.

Laboratory experiments show that static Young's moduli E_s are always less than dynamic Young's moduli [*van Herdeen*, 1987; *Cheng and Johnston*, 1981]. *Cheng and Johnston* [1981] determined that the E_s/E_d ratio increases with depth as microcracks close and reduce in number. For granite and sandstones, they found ratios E_s/E_d of about 0.5 at atmospheric pressure which approach unity at high pressures. However, for high crack porosity, they noticed that the E_s/E_d ratio can become as low as 0.1. The dike intrusion studied here occurred in the shallowest part of the edifice, which is made of thin vesiculated lava flows, separated by layers of scorias. It is weathered by heavy rains and volcanic activity. Thus we will suppose that $E_s/E_d = 0.25$, giving a value of E_s = 5 GPa. This Young's modulus is close to the values (2.4-3.6 GPa) found by *Rubin and Pollard* [1987] from estimates of a dike thickness at Kilauea volcano, Hawaii. It is also similar to the Young's modulus determined for the uppermost part of the Icelandic crust (7.2 MPa) by *Gudmundsson* [1988].

3.1.2. Geometry and position of the source of displacements. The volume of lava emitted for this eruption is estimated to be 17×10^6 m^3 [*Lénat et al.*, 1989a]. However, geodetic and clinometric data [*Lénat et al.*, 1989a, Figure 8] show that the eruption was not associated with any deflation over the Enclos Fouqué caldera. This can be explained if the reservoir from which the magma was extracted is deep enough so that the resulting ground deformations are negligible. Using Mogi's model, less than 1 cm of subsidence would occur if the 17×10^6 m^3 of lava came from a spherical reservoir located deeper than 19 km. It is also possible that the reservoir is not so deep but is not spherical. For instance, for a given volume of withdrawn magma, a sill-like reservoir would produce a smaller volume of deflation than a spherical reservoir [*Delaney and McTigue*, 1994]. Similarly, a vertically elongated ellipsoidal reservoir would produce less vertical displacement than a spherical one [*Davis*, 1986]. Vertical and horizontal ground displacements also tend to be smaller for volcanoes with a prominent topography than for flat ground surfaces [*Cayol and Cornet*, 1998]. We will assume that the recorded displacements result only from shallow perturbations of the volcanic edifice, and we will not consider the deflation of a deeper magma chamber.

Eruptive fissures produced during this event have a N195°E azimuth for the first episode and a N205°E azimuth for the second episode (Figure 2a). They are radial to the central craters and have en echelon arrangement. These fissures are located along a trend averaging N165°E. Following *Delaney and Pollard* [1981], it will be supposed that the en echelon pattern of the eruptive fissures is caused by a rotation of the minimum principal regional stress near the ground surface. At depth, these fissures probably coalesce to form a single dike oriented N165°E, circumferential to the central craters. This hypothesis is consistent with the fan-shaped pattern of horizontal displacements shown by photogrammetry.

Approximately 2 hours before each eruptive episode, seismic swarms were recorded to the southwest of Dolomieu crater [*Lénat et al.*, 1989a, Figures 4 and 6]. Then, seismicity decreased before starting again at the eruption onset. It is our hypothesis that these seismic swarms correspond to the initiation (first episode) and the reopening (second episode) of a macroscopic dike and that the subsequent decrease of seismicity corresponds to the quasi-static propagation of this dike toward the ground surface. For the preliminary model, we assume that the dike starts from the top of the seismic

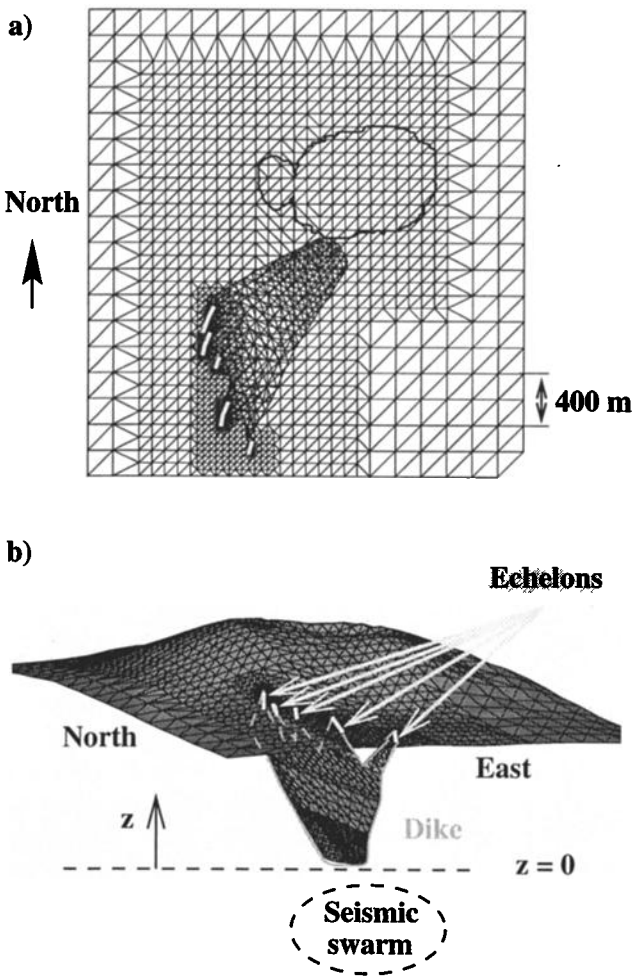

Figure 3. Geometry and computational mesh for the dike modeled using the three-dimensional mixed boundary element method. The dike starts from an area corresponding to the seismic swarm recorded before the eruption. This dike enlarges as it approaches the ground surface. Near this surface, it divides into five en echelon segments. The strike of the deep dike is N165°E, and the average height is 1100 m. Only a portion of the complete mesh is represented in the Figure. This portion corresponds to the area used for representing photogrammetric data and computed displacement vectors. (a) Map view. (b) Oblique perspective view.

swarm, at a depth of approximately 1000 m above sea level, directly below the southwestern rim of Dolomieu crater. According to this hypothesis, the dike propagated upward for an hour at an average speed of 0.3 m/s. This speed is similar to that estimated by *Toutain et al.* [1992] for the April 18, 1990, dike intrusion of Piton de la Fournaise (0.21 m/s).

The length of the upper part of the seismic swarm is about 800 m. However, it is likely that errors in the earthquakes locations show it to be larger than reality. Therefore we will suppose that the initial length of the dike is 400 m. The length of the dike near the ground surface is assumed to correspond to the distance of 1000 m over which eruptive fissures span. These assumptions lead to a dike that enlarges upon propagation, which corresponds to the geometry observed for artificial hydraulic fractures. The dip of this dike is approximately 45°. This dip is consistent with the similar amplitudes of the horizontal and vertical displacements observed by photogrammetry.

The features of the model described above are summarized in Figure 3. A mesh of the ground surface (Figure 3) is constructed from a digital elevation model provided by the French Institut Géographique National. This mesh is made of triangular elements with size gradually increasing, such that their surface goes from 0.125×10^3 m near the eruptive fissures to 80×10^3 m near the edges of the mesh. To minimize edge effects to 4% [*Cayol,* 1996], the ground surface mesh extends for 12 km north-south and for 8 km east-west. This mesh completely encloses the Enclos Fouqué caldera.

3.1.3. Overpressure model. The second photogrammetric survey took place 4 months after the end of the eruption. We postulate that thermal contraction, stress changes in the host rock and weathering during these 4 months had little effect on the shape of the dike and that this shape is related to the stresses acting on it at the end of the eruption. We assume that this shape corresponds to a fracture filled with liquid magma at static equilibrium [*Weertman,* 1971]. The overpressure ΔP (also called driving pressure) that maintains the dike open results from the difference between the magma pressure P and the regional stress S normal to the dike walls, $\Delta P = P - S$. The reference depth $z = 0$ of the vertical z axis is taken at the bottom of the dike, 1000 m above sea level (Figure 3b).

3.1.3.1. Magma pressure determination: In the magma at static equilibrium, the hydrostatic pressure gradient is

$$\frac{\partial P}{\partial z} = -\rho_m(z)\, g, \tag{4}$$

where $\rho_m(z)$ is the magma density and g is the acceleration of gravity. At the end of the eruption, the explosive activity was weak and lava was flowing in lava tubes. This observation indicates that the amount of gas was low at that time. We then assume that vesiculation in the dike was negligible, which implies that the density of lava can be considered constant over the height of the dike $\rho_m(z) = \rho_m$.

At depth z, the pressure can be written

$$P(z) = -\rho_m\, g\, z + P_0, \tag{5}$$

where P_0 is the magma pressure at the base of the dike. Calculation of this pressure is critical. It results from the weight of the magma column and the overpressure at the feeder P_{01}. The height of the magma column H is estimated to be 1100 m. For the 1983-1984 eruption, no reliable gravity measurements are available.

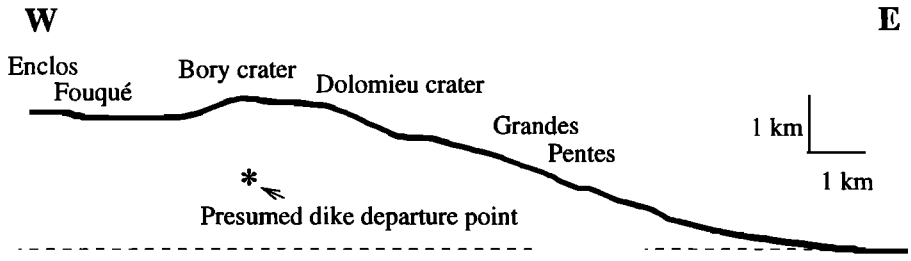

Figure 4. West-east profile of Piton de la Fournaise volcano. In order to calculate gravitational stresses using an axisymmetrical model, only the western part of the edifice is considered.

However, for a similar eruption in June 1985, gravity measurements showed that the dike emplacement was associated with a positive gravity variation [*Lénat et al.*, 1989b]. This indicates that the density of dikes is greater than the density of the surrounding volcanic materials. This density was previously estimated to be 2500 kg/m^3. Thus we will suppose that the magma density is 2650 kg/m^3. Similarly, gravity data and seismic modeling of Hawaii [*Broyles et al.*, 1979; *Zucca et al.*, 1982] and Iceland [*Palmason*, 1971] have shown that, within a few kilometers from the ground surface, the density of unvesiculated magma is larger than the density of the surrounding rock. With those assumptions, the magma pressure at the base of the dike is written

$$P_0 = \rho_m \; g \; H + P_{01} = 29 \text{ MPa} + P_{01}. \qquad (6)$$

Finally, the magma pressure is linearly varying along the dike according to the following equation:

$$P(z) = (-0.026 \; z + 29) \text{ MPa} + P_{01}. \qquad (7)$$

3.1.3.2. Regional stress estimation: The regional stress field results from gravitational stresses, regional tectonic stresses, thermal stresses, etc. Regional tectonic stresses are assumed not to have a significant influence on stresses in the uppermost part of the volcano. Thermal stresses are also neglected, and we will assume that the dominant part of the regional stress field comes from gravitational forces. Calculation of gravitational stresses is not straightforward. Indeed, gravitational stresses result from the progressive growth of the volcano (dike intrusions, superpositions of lava flows and gravitational sliding). A proper calculation of gravitational stresses requires many assumptions about this growth. As a first approximation of the regional stress field, we simply apply gravitational forces to an elastic, homogeneous, isotropic volcanic edifice that was initially stressfree.

This calculation is performed using a finite element code (ZéBuLoN [*Besson et al.*, 1996]). The volcano is assumed to be axisymmetrical. For Piton de la Fournaise volcano, this geometrical approximation is coarse as the volcano has a horseshoe shaped caldera, such that the eastern flank of the volcano is steeply sloping down to the sea, whereas the western flank is sloping up to the walls of the Enclos Fouqué caldera (Figure 4). Because the presumed starting point of the dike is located beneath the western part of the central craters, the western part of the west-east profile is used for constructing a radial crosssection in the axisymmetrical model. In order to avoid edge effects, the bottom and the outer edges are located at distances that represent approximately 5 times the size of the study area (2750 m high and 3000 m deep). Horizontal displacements along the axis of symmetry are zero, and vertical displacements are unconstrained. The bottom of the grid is fixed horizontally as well as vertically. The outer edge is free vertically and fixed horizontally to account for the finite size of the Earth's surface.

Principal stress directions and magnitudes from the gravitational model are plotted on Figure 5. The maximum principal stress is vertical except for the shallowest 300 m where it becomes parallel to the ground surface. The minimum and intermediate principal stresses have subequal amplitudes 300 m below the ground surface. Therefore it can be assumed that deeper than 300 m the stress field is isotropic in the horizontal plane. It should also be noticed that the intermediate principal stress σ_2 is a nonzero compressive horizontal stress at the ground surface of the volcanic edifice. Similar nonzero compressive stresses were already found for ridges by *Savage and Swolfs* [1986].

Assuming that the dike propagated circumferentially with a dip of 45°, amplitudes of the principal stress along this dike path are represented in Figure 6. For the first 800 m (from the initiation point upward), principal stresses decrease almost linearly. Thus they will be approximated as varying linearly, with a slope corresponding to the variation of stresses in the deepest 800 m.

Calculation of normal stresses exerted by this regional stress field on a circumferential dike with a 45° dip gives

$$S(z) = (-0.014 \; z + 19) \text{ MPa}. \qquad (8)$$

3.1.3.3. Overpressure estimation: Finally, the dike overpressure can be approximated as the following linear variation

$$\begin{aligned} \Delta P(z) &= P(z) - S(z) \\ &= (-0.012 \; z + 10 + P_{01}) \text{ MPa}. \end{aligned} \qquad (9)$$

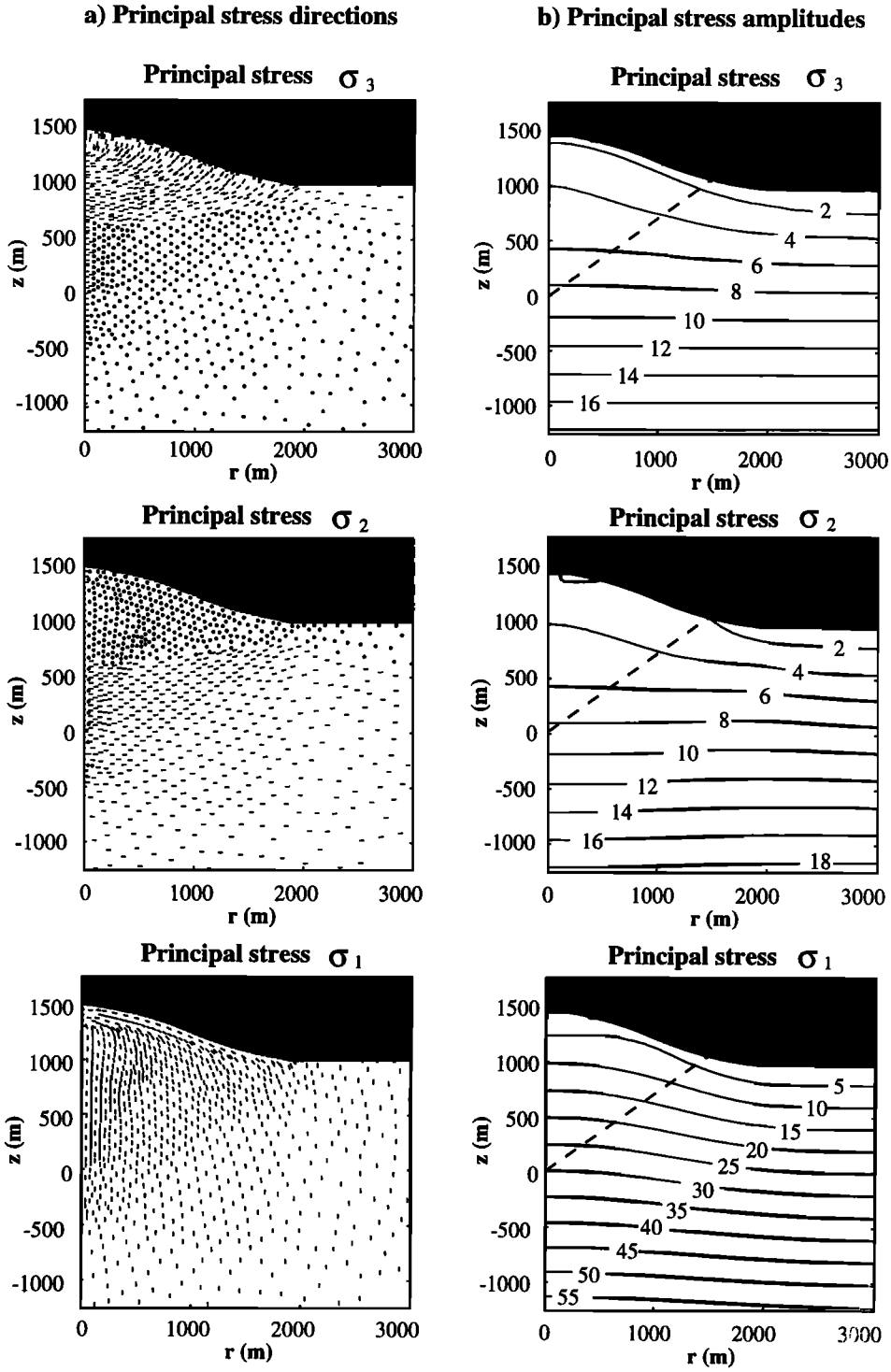

Figure 5. Regional stress field resulting from a gravitational stress model. (a) Principal stress directions ($\sigma_3 < \sigma_2 < \sigma_1$). Principal directions in the (r, z) plane are plotted as short lines, whereas principal directions along θ are plotted as small circles. (b) Principal stress amplitudes. Solid lines represent isovalues (in megapascals). The dashed inclined line which starts from $z = 0$ represents the presumed dike path.

3.2. Best Model Determination

3.2.1. Case I. In (9), the overpressure at the base of the dike is undefined. We estimate this overpressure by minimizing the weighted mean squares χ^2 on the residuals of displacements, defined as

$$\chi^2 = \frac{1}{N_{\text{phot pts}}} \left[\sum_{\text{phot pts}} \frac{(u^{\text{obs}} - u^{\text{mod}})^2}{\sigma^2} \right],$$

where u^{obs} and u^{mod} are the amplitudes of the observed and modeled displacement vectors, respectively, σ is the uncertainty (3 cm) on the observed displacements, and $N_{\text{phot pts}}$ is the number (125) of observation points. A 14-MPa overpressure at the base of the dike minimizes the weighted mean squares ($\chi^2 = 10.7$) which yields

$$\Delta P(z) = (-0.012\ z + 14)\ \text{MPa}. \quad (10)$$

With this overpressure model, the directions of the modeled displacements (Figure 2b) are similar to the directions of the displacements observed by photogrammetry with fan-shaped orientations around the eruptive fissures. This shows that the presumed dike geometry is close to reality. However, modeled horizontal displacements near the eruptive fissures are smaller than the observed displacements. Also, the vertical swell of the northern side of the summit cone is not explained nor are downward displacements to the southeast of Dolomieu crater. A map view (Plate 1a) of the ground surface displacements directed N110°E, perpendicularly to the dike segments (average direction of N200°E), shows that the maximum opening of the eruptive fissures is only 10 cm, when field observations indicated an opening of the dike segments of the order of a meter at the end of the eruption (H. Delorme, personal communication, 1995).

These discrepancies can be explained by the Young's modulus being too small or the magnitude of the overpressure gradient being too large. If the material was stiffer, with, for instance, a Young's modulus of 10 GPa, corresponding to the case of an intact rock mass at atmospheric pressure ($E_s/E_d = 0.5$), a good agreement between modeled displacements and photogrammetric data would be found for $\Delta P(z) = (-0.012\ z + 20)$ MPa. With this Young's Modulus, the maximum dike opening would only be 50 cm. This remains lower than the observed dike opening. Moreover, such a high Young's modulus is very unlikely. Thus it is more likely that the magnitude of the overpressure gradient is lower that the one supposed in this first model.

3.2.2. Case II. As a next step, both the overpressure gradient and the overpressure at the base of the dike are adjusted to fit the eruptive fissures openings and minimize the weighted mean squares of the residuals of displacements. An overpressure of

$$\Delta P(z) = (-0.002\ z + 7)\ \text{MPa} \quad (11)$$

gives the best fit ($\chi^2 = 12.4$) to photogrammetric data (Figure 2c) with larger horizontal displacements near the eruptive fissures. Ground surface displacements directed perpendicularly to the dike segments (Plate 1b) show that the eruptive fissures are now opened by a maximum amount of 90 cm, giving a better fit of the field observations.

Representation of residuals (Figure 7) shows that some horizontal displacements remain unexplained to the south of the central cone, as well as the swelling of the northern side of the central cone. No geophysical data (apart from the displacement vectors observed by photogrammetry) or field observation allow us to postulate structures other than the one modeled. When analyzing deformation data only, solutions are nonunique; therefore it is speculative to introduce new structures without any other geophysical or geological constrains to the model. It is also possible that the vertical displacements to the north of the central cone contain an unknown error.

In order to quantify the differences between modeled displacements and photogrammetric data, relative errors are calculated at the photogrammetric points,

$$\text{Err}\, u_{\text{dir}}(\%) = \frac{\sum_{\text{phot pts}} \left| u^{\text{obs}}_{\text{dir}} - u^{\text{mod}}_{\text{dir}} \right|}{\sum_{\text{phot pts}} \left| u^{\text{obs}}_{\text{dir}} \right|} \times 100, \quad (12)$$

where u_{dir} (dir $= e, n,$ or v) stands for either eastward, northward, or vertical displacements. Although the visual fit between observed and modeled displacements is satisfactory, relative errors are found to be 38% on eastern components, 45% on northern components, and 61% on vertical components. This reflects that the photogrammetric data were only explained to the first order.

3.2.3. Comparison with the case of a flat topography. One of the advantages of the 3-D mixed BE method is that realistic topographies can be incorporated into models. In order to quantify the topographic effects on the modeled displacements, the same dike model as case II was used with a flat ground surface topography (half-space model) located at the average elevation of the photogrammetric points (2433 m). The dike segments are extended or shortened in order to intersect this surface.

In order to estimate the difference between displacements calculated for a flat and for a realistic ground surface, mean relative differences are calculated as follows:

$$D\, u_{\text{dir}}(\%) = \frac{\sum_{\text{phot pts}} \left| u^{\text{topo}}_{\text{dir}} - u^{\text{plan}}_{\text{dir}} \right|}{\sum_{\text{phot pts}} \left| u^{\text{topo}}_{\text{dir}} \right|} \times 100, \quad (13)$$

where u_{dir} (dir $= e, n,$ or v) represents either eastern,

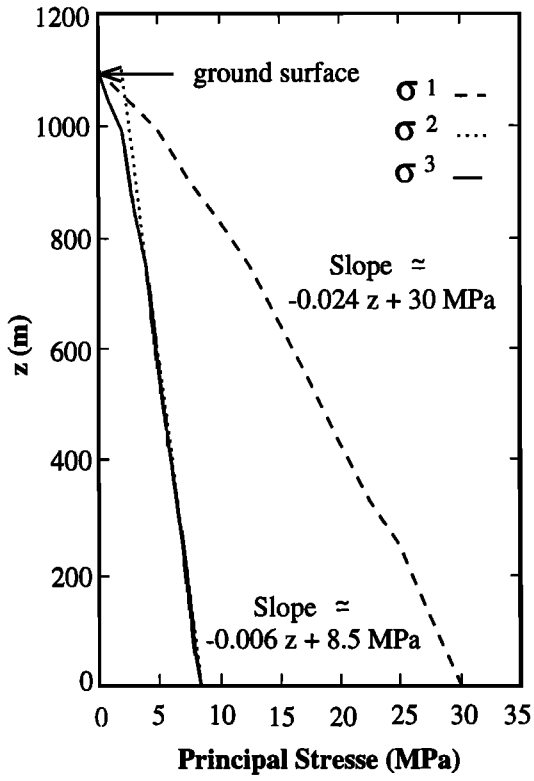

Figure 6. Principal stress amplitudes as a function of depth along the presumed dike path, determined from the regional stress model in Figure 5. Null elevation corresponds to the dike starting point.

northern, or vertical displacements. It is found that topography has the largest influence on northern displacements (27% of relative difference), whereas 16% and 17% of relative difference are found on eastern and vertical displacements, respectively. Moreover, this flat ground surface model leads to larger weighted mean squares ($\chi^2 = 15.1$) and a smaller eruptive fissures opening (60 cm) than the realistic ground surface model. With a flat ground surface, an overpressure of $0.002\,z+4$ MPa (positive gradient) is required to get a 90-cm opening of the fissures, and the weighted mean squares are the largest ($\chi^2 = 16.9$).

3.3. Discussion

The fairly good fit between photogrammetric data and displacements calculated for a model consistent with field and geophysical observations indicates that the behavior of the volcano at the timescale of a dike intrusion is compatible with an elastic rheology.

The dike overpressure that best explains photogrammetric data and fracture opening has a vertical gradient amplitude 6 times smaller (0.002 MPa/m) than that (0.012 MPa/m) estimated from the gravitational loading of an elastic volcanic edifice. This low gradient can be explained either by a smaller amplitude of the magma pressure gradient $|\partial P/\partial z|$ or by a larger amplitude of the regional stress gradient $|\partial S/\partial z|$. A lower amplitude of the magma pressure gradient would require a lower magma density of 1700 kg/m^3 to account for an overpressure gradient with a 0.002-MPa/m amplitude. As mentioned before, this is incompatible with the gravity observations. The other possibility is that the regional stresses gradient has a larger magnitude. In fact, if the regional stress tensor is isotropic with diagonal terms equal to the weight of the overlying rocks, the overpressure gradient has a 0.002-MPa/m magnitude and thus corresponds to the value determined from the modeling of ground surface displacements. This quasi-isotropic state of stress implies that the stresses in the volcano are not that of an elastic edifice loaded by gravitational forces merely as supposed in Figure 5. However, the state of stress is consistent with the assumptions of *Dieterich* [1988] and *Chadwick and Dieterich* [1995] for the basaltic shield volcanoes of Kilauea and Galapagos. Indeed, following *Anderson*'s [1936] hypothesis, they postulated that dikes intrude perpendicular to the minimum principal stress, and, with time, increase this stress and reduce deviatoric stresses, moving the volcano toward a state of isotropic stress. At Piton de la Fournaise, observations of surface fractures [*Lénat and Bachèlery,* 1990] indicate that intrusions in the summit area account for a significant portion of the volume of the central cone. Inversion of arrival times of earthquakes [*Nercessian et al.,* 1996], as well as gravity studies [*Rousset et al.,* 1989] show the presence of dense rocks beneath the central craters. These dense rocks can be attributed to the numerous intrusive events that occurred in the summit area of the volcano. Therefore the state of stress we determined could result from the frequent repetition of dike intrusions.

Sustained long-term dike intrusions have to be accommodated by the edifice. Stresses accumulated by successive diking events can be relaxed by two mechanical processes. The first is the development of plasticity, and the second is the localization of deformations along fracture zones. On Hawaiian volcanoes, it is recognized that repeated intrusions are accommodated by large-scale faulting of the volcano's flanks [*Swanson et al.,* 1976; *Dieterich,* 1988]. At Piton de la Fournaise, eruptive fissures cluster along two fracture zones trending N10°E and N170°E (Figure 1), and the central cone is elongated along the west-east direction (Figure 1b). Moreover, the distribution and tectonic characteristics of summit fissures seemingly reflect a tensional mechanism involving an eastward sliding of the eastern side of the volcano (Grand Brûlé structure) [*Lénat et al.,* 1989c]. The quasi-isotropic state of stress supports the hypothesis that basaltic shield volcanoes are in critical equilibrium, so that stresses within the edifice are close enough to the stresses in a standing column of magma to permit eruptions when an overpressure occurs at depth and close enough to critical levels for intrusive events to result in sliding along fault.

Since the regional state of stress we found is quasi-isotropic, the dike propagation path cannot be explained by this regional stress. However, the dike path could

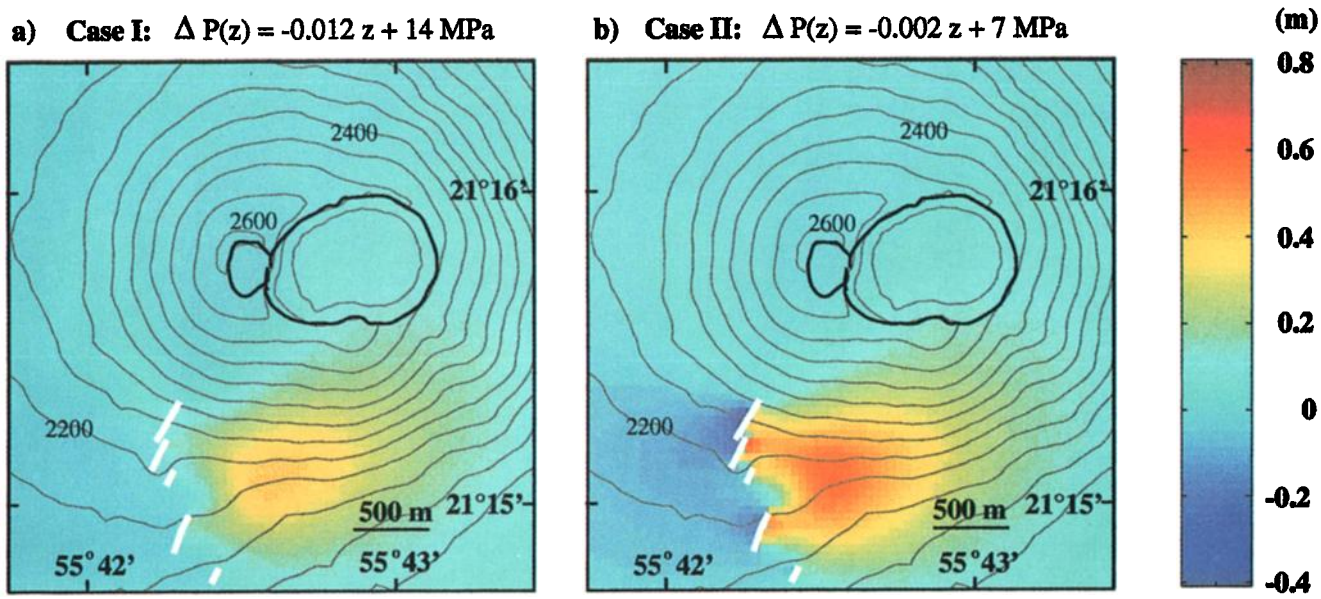

Plate 1. Map view of N110°E directed ground displacements for two different overpressure models. Elevation contours are every 50 m. Eruptive fissures are in white. (a) Case of a dike with an overpressure of $\Delta P(z) = (-0.012z + 14)$ MPa. At the ground surface, the maximum opening of the dike segments is 10 cm. (b) Case of a dike with an overpressure of $\Delta P(z) = (-0.002z + 7)$ MPa. At the ground surface, dike segments are open by as much as 90 cm.

have been influenced by a shallow pressurized magma reservoir [*Anderson,* 1936; *Chevallier and Verwoerd,* 1988], by the shape of this reservoir [*Chadwick and Dieterich,* 1995], by heterogeneities in mechanical properties, or by heterogeneities in the regional stress field; which depends on the mechanical history of the volcano. Thermal stresses might also have played a role.

Quantitatively, the 3-D mixed BE model is more successful in explaining the photogrammetric data than the dislocations model [*Zlotnicki et al.,* 1990]: near the eruptive vents, the mixed BE model accounts for the large horizontal displacements better than the dislocation model, and northeast of the vents, the mixed BE model accounts very well for the rapid decrease of horizontal displacements, 50% over 1000 m, while the dislocation model only gives a 20% decay over 1000 m. Furthermore, the dike we determined, although geometrically more complex, is physically simpler and closer to field observations. It is a fan-shaped planar dike that enlarged upon propagation toward the surface and divided into echelons, whereas the geometry modeled using dislocations is a rectangular dike, 1300 m wide at the base which is intersected by two quasi-vertical dikes 300 m high. The three dikes do not intersect the ground surface as they are located 300 m below the flat ground surface. Additionally, the mixed BE model has two features the dislocation model lacks: it takes topography into account avoiding the introduction of artifacts when searching for the best fitting model and, most importantly, it determines stress distributions improving our knowledge of the stress field inside a volcano.

Finally, we have seen that for Piton de la Fournaise use of a half-space model (flat ground surface) can lead to a different interpretation of deformation data than when taking the realistic topography into account. This approximation of the Earth's surface geometry can mislead the interpretations. For instance, when the ground surface was considered flat, the overpressure was found to have a positive gradient, whereas the gradient was found to be negative when the realistic topography was taken into account.

4. Conclusions

A three-dimensional mixed boundary element method has been applied to the analysis of ground surface displacements associated with the 1983-1984 eruption of Piton de la Fournaise. Modeling of a dense set of photogrammetric data has shown that both episodes of the eruption were fed by a single dike oriented N165°E at depth. This dike is 1100 m high; it enlarged upon propagation to reach a length of 1000 m near the ground surface where it divided into segments which rotated to become radial to the central craters when they intersected the ground surface.

At the timescale of an intrusion, the volcano appears to behave elastically. Determination of the dike overpressure indicates that the state of stress in the volcano is not compatible with an elastic edifice merelv loaded by gravitational forces. Instead, stress gradients inside the volcanic edifice are found to be very close to isotropic such that the diagonal terms of the stress tensors are equal to the weight of the overlying rocks. This can be attributed to an increase in horizontal stresses due to repeated dike intrusions. This inference is supported by seismic and gravity studies, which have shown

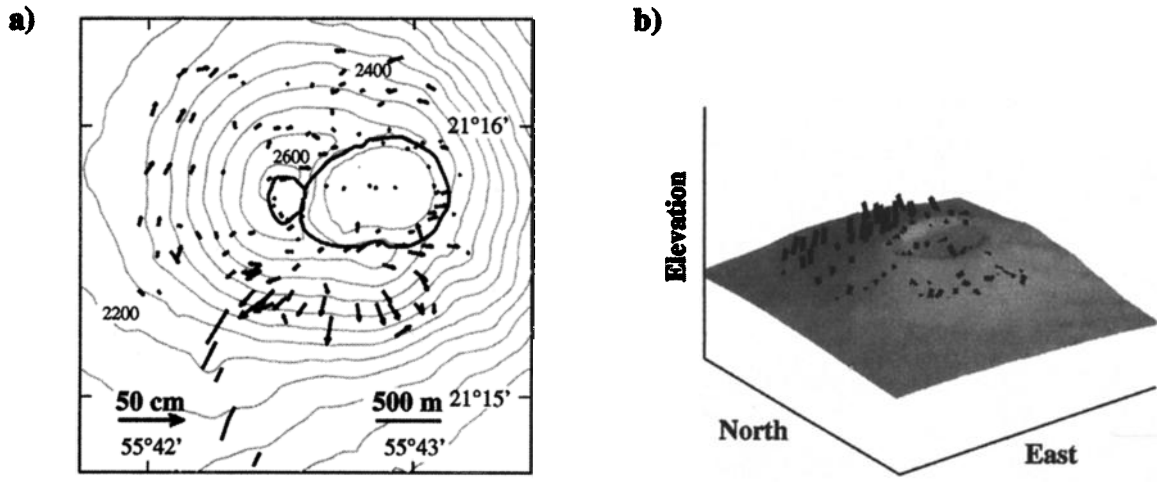

Figure 7. Residuals between the displacements observed by photogrammetry and the displacements computed by the mixed BE method for a dike with an overpressure $\Delta P(z) = -0.002z + 7$ MPa. (a) Map view. Elevation contours are every 50 m. (b) Oblique perspective view.

that the summit cone of Piton de la Fournaise is made of dense rocks.

Finally, comparing with a half-space model, we have shown that modeling a realistic topography avoids errors of 27%, 16%, and 17% on the northern, eastern, and southern components of displacements, respectively. We also saw that neglecting topography could significantly affect our interpretation of the ground surface displacements.

Acknowledgments. This research was funded in part by CNRS-ECOTEC (ARC Geothermie des Roches Fracturées) and by the 4th European Community program for natural hazards reduction. Ross Stein, Paul Delaney, William Chadwick, and John Dvorak helped improve this manuscript. We also thank Maurizio Bonafede, Agust Gudmundsson, and James Dieterich for useful comments and discussions. The help of Francois Beauducel with Matlab is also greatly aknowledged.

References

Albarède, F., Residence time analysis of geochemical fluctuations in volcanic series, *Geochim. Cosmochim. Acta, 57*, 615-621, 1993.

Anderson, E. M., The dynamics of the formation of cone sheets, ring-dikes and cauldron subsidences, *R. Soc. of Edinburgh, 56*, 128-163, 1936.

Besson, J., R. Foerch, and G. Cailletaud, ZéBuLon Version 7, Centre des Mat., École Nat. Supér. des Mines de Paris, Evry, 1996.

Broyles, M. L., W. Suyenaga, and A. S. Furumito, Structure of the lower east rift zone of Kilauea volcano, Hawaii, from seismic and gravity data, *J. Volcanol. Geotherm. Res., 5*, 317-336, 1979.

Bureau H., F. Pineau, N. Metrich, M. Semet and M. Javoy, A melt and fluid inclusion study of the gas phase at Piton de la Fournaise volcano (Réunion Island), *Chem. Geol.*, in press, 1998.

Cayol, V., Analyse élastostatique tridimensionnelle du champ de déformations des édifices volcaniques par éléments frontières mixtes, thèse de doctorat, Univ. de Paris VII, Paris, 1996.

Cayol, V., and F. H. Cornet, 3D mixed boundary elements for elastic deformation field analysis, *Int. J. Rock Mech. Min. Sci. Geomech. Abstr., 34*, 275-287, 1997.

Cayol, V., and F. H. Cornet, Effects of topography on the interpretation of the deformation field of prominent volcanoes - Application to Etna, *Geophys. Res. Lett.*, in press, 1998.

Chadwick, W. W., and J. H. Dieterich, Mechanical modeling of circumferential and radial dike intrusion on Galapagos volcanoes, *J. Volcanol. Geotherm. Res., 66*, 37-52, 1995.

Cheng, C. H., and D. H. Johnston, Dynamic and static moduli, *Geophys. Res. Lett., 8*, 39-42, 1981.

Chevallier, L., and W. J. Verwoerd, A Numerical model for the mechanical behavior of intraplate volcanoes, *J. Geophys. Res., 93*, 4182-4198, 1988.

Corre, P., and P. Giraudin, Une expérience de surveillance photogrammétrique: la route d'accès du tunnel routier de Fréjus, *Bull. Inf. IGN., 45*, 23-31, 1982.

Crouch, S. L., Solution of plane elasticity problems by the displacement discontinuity method. *Int. J. Numer. Methods Eng., 10*, 301-343, 1976.

Curran, J. H., B. T. Corkum, and S. Shah, *COMPUTE^{3D} BEM*, version 2.23, Rock Eng. Group, Dep. of Civ. Eng., Univ. of Toronto, Ont., Canada, 1994.

Davis, P. M., Surface deformation due to inflation of an arbitrarily oriented triaxial ellipsoidal cavity in an elastic half-space, with reference to Kilauea volcano, Hawaii, *J. Geophys. Res., 91*, 7429-7438, 1986.

Delaney, P. T., and D. F. McTigue, Volume of magma accumulation or withdrawal estimated from surface uplift and subsidence, with application to the 1960 collapse of Kilauea volcano, *Bull. Volcanol., 56*, 417-424, 1994.

Delaney, P. T., and D. D. Pollard, Deformation of host rocks and flow of magma during growth of minette dikes and breccia-bearing intrusions near Ship Rock, New Mexico, *U.S. Geol. Surv. Prof. Pap., 1202*, 1202-1263, 1981.

Diering, T. A. C., Further developments of the Boundary Element Method with applications in mining, M.Sc. thesis, Univ. of the Witwatersrand, Johannesburg, South Africa, 1981.

Dieterich, J. H., Growth and persistence of Hawaiian volcanic rift zones, *J. Geophys. Res.*, *93*, 4258-4270, 1988.

Dieterich, J. H., and R. W. Decker, Finite element modeling of surface deformation associated with volcanism, *J. Geophys. Res.*, *80*, 4094-4102, 1975.

Gudmundsson, A., Effect of tensile stress concentration around magma chamber on intrusion and extrusion frequencies, *J. Volcanol. Geotherm. Res.*, *35*, 179-194, 1988.

Hill, D. H., and J. J. Zucca, Geophysical constraints on the structure of Kilauea and Mauna Loa volcanoes and some implications for seismomagmatic processes, *U.S. Geol. Surv. Prof. Pap.*, *1350*, 903-917, 1987.

Lachat, J. C., and J. O. Watson, Effective numerical treatment of boundary integral equations: A formulation for three-dimensional elastostatics, *Int. J. Numer. Methods Eng.*, *10*, 991-1005, 1976.

Lénat, J. F., and P. Bachèlery, Structure and dynamics of the central zone of Piton de la Fournaise volcano, in *Le volcanisme de la Réunion - Monographie*, pp. 257-296, CRV, Clermont-Ferrand, 1990.

Lénat, J. F., P. Bachèlery, A. Bonneville, P. Tarits, J. L. Cheminée, and H. Delorme, The December 4, 1983, to February 18, 1984 eruption of Piton de la Fournaise (La Réunion, Indian Ocean): Description and interpretation, *J. Volcanol. Geotherm. Res.*, *36*, 87-112, 1989a.

Lénat, J. F., P. Bachèlery, A. Bonneville, and A. Hirn, The beginning of the 1985-1987 eruptive cycle at Piton de la Fournaise (La Réunion); New insights in the magmatic and volcano-tectonic systems, *J. Volcanol. Geotherm. Res.*, *36*, 209-232, 1989b.

Lénat, J. F., P. Vincent, and P. Bachèlery, The off-shore continuation of an active basaltic volcano: Piton de la Fournaise (Réunion Island, Indian Ocean); Structural and geomorphological interpretation from Sea Beam mapping, *J. Volcanol. Geotherm. Res.*, *36*, 1-36, 1989c.

McTigue, D. F., Elastic stress and deformation near a finite spherical magma body: Resolution of the point source paradox, *J. Geophys. Res.*, *92*, 12,931-12,940, 1987.

McTigue, D. F., and P. Segall, Displacements and tilts from dip-slip faults and magma chambers beneath irregular surface topography, *Geophys. Res. Lett.*, *15*, 601-604, 1988.

Mogi, K., Relations between the eruptions of various volcanoes and the deformation of the ground surfaces around them, *Bull. Earthquake Res. Inst. Univ. Tokyo*, *36*, 99-134, 1958.

Murkherjee, S., and M. Marjoria, On the efficiency and accuracy of the Boundary Element Method and the Finite Element Method, *Int. J. Numer. Methods Eng.*, *20*, 515-522, 1984.

Nercessian, A., A. Hirn, J. C. Lépine, and M. Sapin, Internal structure of Piton de la Fournaise volcano from seismic wave propagation and earthquake distribution, *J. Volcanol. Geotherm. Res.*, *70*, 123-143, 1996.

Okada, Y., Surface deformation due to shear and tensile faults in a half-space, *Bull. Seismol. Soc. Am.*, *75*, 1135-1154, 1985.

Palmason, G., Crustal structure of Iceland from explosion seismology, *Soc. Sci. Isl.*, *40*, 187 pp., 1971.

Pollard, D. D., P. T. Delaney, W. A. Duffield, E. T. Endo, and A. T. Okamura, Surface deformation in volcanic rift zones, *Tectonophysics*, *94*, 541-584, 1983.

Rousset, D., A. Lesquer, A. Bonneville, and J. F. Lénat, Complete gravity study of Piton de la Fournaise volcano, Réunion Island, *J. Volcanol. Geotherm. Res.*, *36*, 37-52, 1989.

Rubin, A. M., and D. D. Pollard, Origins of blade-like dikes in volcanic rift zones, *U.S. Geol. Surv. Prof. Pap.*, *1350*, 1449-1470, 1987.

Sapin, M., A. Hirn, J. C. Lépine, and A. Nercessian, Stress, failure and fluid flow deduced from earthquakes accompanying eruptions at Piton de la Fournaise volcano, *J. Volcanol. Geotherm. Res.*, *70*, 145-167, 1996.

Savage, W. Z., and H. S. Swolfs, Tectonic and gravitational stress in long symmetric ridges and valleys, *J. Geophys. Res.*, *91*, 3677-3685, 1986.

Swanson, D. A., W. A. Duffield, and R. S. Fiske, Displacement of the south flank of Kilauea volcano: The result of forceful intrusion of magma into rift zones, *U.S. Geol. Surv. Prof. Pap.*, *963*, 39 pp., 1976.

Toutain, J. P., P. Bachèlery, P. A. Blum, J. L. Cheminée, H. Delorme, L. Fontaine, P. Kowalski, and P. Taochy, Real time monitoring of vertical ground deformations during eruptions at Piton de la Fournaise, *Geophys. Res. Lett.*, *19*, 553-556, 1992.

van Heerden, W. L., General relations between static and dynamic moduli of rocks, *Int. J. Rock Mech. Min. Sci. Geomech. Abstr.*, *24*, 381-385, 1987.

Weertman, J., Theory of water-filled crevasses in glaciers applied to vertical magma transport beneath oceanic ridges, *J. Geophys. Res.*, *76*, 1171-1183, 1971.

Zeller, S. O., and D. D. Pollard, Boundary conditions for rock fracture analysis using boundary element method, *J. Geophys. Res.*, *97*, 1991-1997, 1992.

Zlotnicki, J., J. C. Ruegg, P. Bachèlery, and P. A. Blum, Eruptive mechanism on Piton de la Fournaise volcano associated with the December 4, 1983, and January 18, 1984, eruptions from ground deformation monitoring and photogrammetric surveys, *J. Volcanol. Geotherm. Res.*, *40*, 197-217, 1990.

Zucca, J. J., D. P. Hill, and R. L. Kovach, Crustal structure of Mauna Loa volcano, Hawaii, from seismic refraction and gravity data, *Bull. Seismol. Soc. Am.*, *72*, 1535-1550, 1982.

V. Cayol and F. H. Cornet, Laboratoire de mécanique des roches, Département de sismologie URA CNRS 195, IPGP, 4 place Jussieu, 75 252 Paris Cedex 5, France (cayol@ipgp.jussieu.fr; cornet@ipgp.jussieu.fr)

(Received June 2, 1997; revised January 7, 1998; accepted January 15, 1998.)